Title:

A new approach to forecasting mountain wave induced clear air turbulence

Short title:

Forecasting mountain wave induced clear air turbulence

Andrew D. Elvidge, Helen Wells, Simon B. Vosper, Jacob C. H. Cheung, St Derbyshire, Debi Turp

Met Office, FitzRoy Road, Exeter, EX1 3PB, UK
Corresponding author:
Andy Elvidge, andy.elvidge@metoffice.gov.uk,
Telephone: 07464493731

Total word count: 6208

A new approach to forecasting mountain wave induced clear air turbulence

Andrew D. Elvidge, Helen Wells, Simon B. Vosper, Jacob C. H. Cheung, St H. Derbyshire, Debi Turp

Abstract

Mountain wave breaking in the lower stratosphere is one of the major causes of atmospheric turbulence encountered in commercial aviation – the cause of mos weather-related aircraft incidents. In the case of clear air turbulence (CAT), ther no visual clues and pilots are reliant on operational forecasts and reports from o aircraft. Traditionally mountain waves have been sub-grid-scale in global foreca models, but recent developments mean that some NWP models (e.g. the UK M Office Unified Model; MetUM) are now able to resolve mountain wave activity explicitly, allowing forecasts of mountain wave induced turbulence with greater accuracy and confidence than previously possible. Despite this, the characterist fine-scale phenomenon of mountain wave breaking is still unlikely to be resolve global models. Accordingly, a modified turbulent kinetic energy (TKE) diagnostic derived, designed to identify regions which are likely to be turbulent. Using the MetUM and automated observations from commercial aircraft, this diagnostic is shown to provide useful forecasts of CAT during three case studies over Greenl and to outperform the current operational Met Office CAT prediction product in so. In a long term, 17-month verification, forecasts based on the TKE diagnostic a turbulence prediction hit rate of 80 % with an accompanying false alarm rate under 40 %; a considerable improvement on the current operational product. Th major implication of this work is that sophisticated global NWP models are now sufficiently advanced that skilful forecasts can be made of mountain wave turbul

2. Methodology and diagnostics

Aircraft encounters with turbulence are the cause of a significant number of occu injuries and, with respect to general aviation, of fatalities and loss of aircraft. Ma such incidents occur at cruise altitudes (typically 8-14 km) and are as a result of presence of clear-air turbulence (CAT), for which there is no visual evidence. In avoidance of CAT, pilots are entirely dependent on operational forecast product Known causes of CAT include strong wind shear (for example, associated with j streams), thunderstorms, and mountain waves (see e.g. Wolff and Sharman, 20

The most severe mountain-induced turbulence is commonly experienced at low in the lee of mountains associated with lee waves, rotors, hydraulic jumps, and body boundary layer separation below mountain-top height (Strauss et al., 2015 Indeed, commercial aircraft typically cruise within the lower stratosphere in part avoid such low-level turbulence. However, under the right conditions, airflow ove mountains can result in the generation of vertically propagating mountain waves which are able to transport energy upwards to levels above the mid-troposphere the stratosphere and as high as the mesosphere. These waves eventually depo their energy, largely via turbulent breakdown as a result of wave steepening or t presence of a critical level due to, for example, rotation of flow direction with hei (Clark and Peltier, 1977; Teixeira and Miranda, 2009).

Mountain wave induced turbulence and the mechanisms responsible for wave breaking is a complex and relatively poorly understood topic, with progress limit part by a lack of available observations. Challenges to direct measurement of mountain turbulence are numerous: by its nature, CAT is difficult to identify and consequently to sample; there are obvious safety concerns related to flying with turbulent regions, particularly in mountainous areas; and capturing the characte spatial and temporal complexity of the turbulence can be problematic. Consequ reports of research aircraft observations of mountain wave turbulence are limited only a handful of studies (Lilly, 1978; Smith, 1987; Wobrock et al., 1997; Jiang a Doyle, 2004; Mobbs et al., 2005; Grubišić et al., 2008; Strauss et al., 2015; Elvi al., 2016). However, automated commercial observations of mountain wave turbulence offer a valuable alternative source of observations; their extensive coverage overcoming to some degree the challenge of sampling.

Using commercial aircraft observations, mountain-wave induced turbulence has shown to pose a hazard to aviation over Greenland (Lane et al., 2009; Shaman 2012) and the Rockies (Wolff and Sharman, 2008). In an analysis of 7 years of reports of turbulence over the Greenland region, Lane et al. (2009) found that th was a report of moderate or greater turbulence on average once every four days Their analysis revealed that the majority of these reports were likely to be assoc with mountain-wave activity and indeed they identified a flow regime (surface cyclones directing easterly or south-easterly flow over Greenland with westerly f aloft) which accounted for approximately 40% of significant turbulence events reported.

threshold value. This is not ideally fit for purpose, as it is the stress divergence r than stress which is associated with wave dissipation.

The realism of this approach is clearly also limited by the simplifications used in drag parametrization schemes. For example, model grid columns are usually tre independently and the waves are typically assumed to be monochromatic and t propagate only in the vertical. Perhaps more crucially, the wave drag is tuned to optimize overall forecast performance, not to provide a realistic representation o waves themselves. A better approach may be to diagnose mountain-wave CAT directly from the model's resolved mountain waves, thus avoiding the need for t crude simplifications used in parametrizations. Recent increases in the resolutio global numerical weather prediction (NWP) models, combined with advances in design of the models may mean that this will be possible in the near future. The of this paper is to provide an initial assessment of a new mountain-wave turbule diagnostic, based on explicitly resolved mountain-wave fields in global NWP forecasts.

2. Methodology and diagnostics

Automated commercial aircraft turbulence reports have been used to assess wh a global NWP model can provide a sufficiently accurate representation of mount waves to forecast mountain-wave CAT. This question is tackled using two complementary approaches: case study analysis and long-term verification. The results section of this paper is divided accordingly. In the case study approach (Section 3), three case studies have been selected. The two most recent of whic (occurring in November 2014 and March 2012) were chosen due to a) the occurrence of multiple moderate to severe turbulence reports over Greenland w a short period of time, and b) analysis charts indicating conditions conducive to mountain wave generation. Note that, for reasons of commercial sensitivity, we unable to provide the date and time of these turbulence encounters. The third ca study is the severe turbulence event in May 2010 examined by Sharman et al. (2012). For the long term verification (Section 4), all recorded aircraft turbulence reports over Greenland during a 17-month period are used to validate turbulenc forecasts.

The observations used are derived from the Global Atmospheric Data Set (GAD produced by automated aircraft measurements from commercial aircraft, and us previously in studies of atmospheric turbulence (e.g. Gill and Stirling, 2012). The measure of turbulence given by these observations is known as the Derived Equivalent Vertical Gust (DEVG). This has been designed to be an aircraft independent measure of turbulence (Truscott, 2000). DEVG is defined as

$$DEVG = \frac{Am|\Delta n|}{V},$$

where $|\Delta n|$ is the peak modulus value of the fractional deviation of the aircraft no acceleration from g (the Earth's gravitational acceleration), m is the total aircraft mass (metric tonnes), V is the calibrated airspeed at the time of occurrence of th

includes two significant recent advances which can be expected to improve the representation of mountain waves:

1. The simulations were run at N768 resolution. This corresponds to a zona length of ~17km at mid-latitudes.

2. The simulations were performed with the latest version of the MetUM dynamical core – ENDGame: Even Newer Dynamics for General Atmosp Modelling of the Environment. This involves a more accurate and numer stable treatment of the equations of motion (Melvin et al, 2010; Wood et 2013) than that available with the New Dynamics dynamical core (Davie al., 2005). Both involve a semi-Lagrangian semi-implicit method to solve compressible deep atmosphere equations, but ENDGame includes a mo consistent treatment of potential temperature advection and improved numerical stability allows for reduced off-centring in the temporal discretization. The latter is known to significantly improve the representa of gravity waves (Shutts and Vosper, 2011) over what is achievable with operational forecasts using the New Dynamics core.

Even at N768 resolution and with an improved representation of gravity wave m it seems unlikely that fine-scale wave overturning regions will be well resolved, if the larger scale wave field is well represented. Using the model's native turbul parametrization to diagnose CAT is therefore likely to underestimate the turbule kinetic energy (TKE); a commonly used diagnostic in the identification of atmosp turbulence (e.g. Strauss et al., 2015). Thus a modified off-line TKE diagnostic fo forecasting mountain-wave CAT is proposed, which is designed to predict turbul when the Richardson number is small, but not necessarily sub-critical. It is deriv via a bulk formula based on the eddy diffusivity for momentum, κ_m, as:

$$TKE = \left(\frac{\kappa_m}{lC} \right)^2 ,$$

where C is a tuneable constant (set to 0.5) and l is the mixing length. The modifi TKE uses a diagnosed eddy diffusivity which assumes a long tail stability functio

$$f(Ri) = \frac{1}{1+10Ri} ,$$

where Ri is the gradient Richardson number. κ_m is then defined as

$$\kappa_m = l^2 S f(Ri) ,$$

where S is the modulus of the vertical wind shear. The use of a long tail stability function provides greater mixing (κ_m) at higher stabilities than used in the turbule parametrization and is therefore more appropriate for situations where the gravi waves are not so well resolved that the convective overturning is explicitly represented. The length scale, l, should arguably relate to the scale of the wave breaking region, though for simplicity a fixed value of 100 m has been assumed

The ENDGame-based TKE forecasts have been compared to the guidance issu the current World Area Forecast Centre (WAFC) London gridded CAT product, predicts CAT based on information from the mountain wave drag scheme in the

Dynamics version of the MetUM and hence contains heavily damped gravity wa
motion.

In the long term verification, the period considered extends from August 2014 (fi
which time ENDGame dynamics and N768 resolution are first available in the
operational MetUM forecast archive) to December 2015. The GADS reports are
confined in the horizontal to the area above Greenland, and to days where surfa
pressure charts indicate conditions conducive to mountain wave activity over
Greenland (i.e. where surface pressure gradients suggest moderate to strong w
across Greenland). Each GADS observation is subject to a thorough quality con
procedure.

Model diagnostics are extracted where they are within one hour, 100 km in the
horizontal and 2 km in the vertical of each GADS observation over Greenland w
low to severe turbulence (DEVG >2) is indicated, and also for a large sample (1
observations where little turbulence (DEVG < 2) is indicated. Limiting the numbe
null reports was necessary for computational considerations, whilst using all the
positive turbulence reports was necessary to provide a worthwhile study. In tota
2606 reports are used. Of these, 16 (0.6 %) were reports of moderate to severe
turbulence, 466 (17.9 %) were light turbulence reports, and the remaining 2124
%) were null reports.

3. Case study verification

3.1 Case 1: Moderate, widespread turbulence

During this case in November 2014, moderate turbulence was experienced by a
aircraft passing over southern Greenland. Consecutive automated DEVG report
indicating light to moderate turbulence occurred at two distinct regions: above s
slopes near Greenland's south west coast (where the peak DEVG observation o
m s^{-1} was reported), and above the central Greenland plateau. Over the plateau
second aircraft flying at lower altitude (~1.5 km lower) also experienced light
turbulence within an hour of the other aircraft's reports. On these two flights,
turbulence was also reported over the Iceland Sea to the east of Greenland, wh
further flights traversing over Greenland and over the sea to the south experienc
no turbulence. The locations of all turbulence and null reports are shown in Figu

Synoptic conditions on this day were characterised by a deep low pressure syst
the south which drove strong south-easterly flow across southern Greenland. As
previously mentioned, such conditions are prevalent when mountain turbulence
experienced over Greenland (Lane et al., 2009). Model horizontal wind vectors
same height and within an hour of the peak turbulence report (PTR) during this
are shown in Figure 1(a). Figure 2 shows vertical profiles of the global model wi
velocity, buoyancy frequency and diagnosed TKE at the closest model grid-poin
the PTR. These profiles show that the atmosphere was stably stratified and so
capable of supporting gravity wave propagation, and that south easterly winds
extended from ~1 km to near cruise altitude. Above ~ 9 km, the wind speed drop

and wind shear in the boundary layer (Figure 2(a)) indicate the potential for wav instability and turbulence. At cruise altitude in the vicinity of the PTR, convective overturning and strong wind shear are also seen. Indeed, the TKE diagnostic (F 1(c)) suggests turbulence over a wider region at cruise altitude. The stagnant, w stable layer at ~11.5 km apparent in Figure 2 is indicative of a wave-induced cri level, a feature associated with the turbulent dissipation of mountain waves. Fur east, another region of wave steepening is apparent, corresponding to the seco region of turbulence diagnosed from the DEVG reports.

Diagnosed TKE at the height of the PTR and mean TKE at this height ±2 km are shown in Figure 1(c,e). Encouragingly, the majority of the turbulence observatio over Greenland lie within the region indicated by the height-averaged TKE as be at risk of turbulence. The westward region of turbulence is precisely forecast, wi high TKE predicted at the location of the PTR (Figures 1(c,d) and 2(b)). Interesti a region at risk of turbulence is predicted to the east of Greenland over the Icela Sea, within which several turbulence reports were located (Figure 1(e)). In this c the diagnostic highlights an unstable region which is close to a synoptic frontal feature.

The closest gridded WAFC CAT forecast (Figure 1(f)) to the PTR on this day wa the 250 hPa level and within an hour of the report. Note that the WAFC CAT for is issued as a dimensionless measure of the potential for turbulence and as suc values cannot be directly compared to the TKE. In this case the WAFC product correctly predicts the potential for turbulence in both observed regions. Howeve TKE diagnostic highlights a more localised region of turbulence than the WAFC diagnostic, providing a more precise and useful forecast.

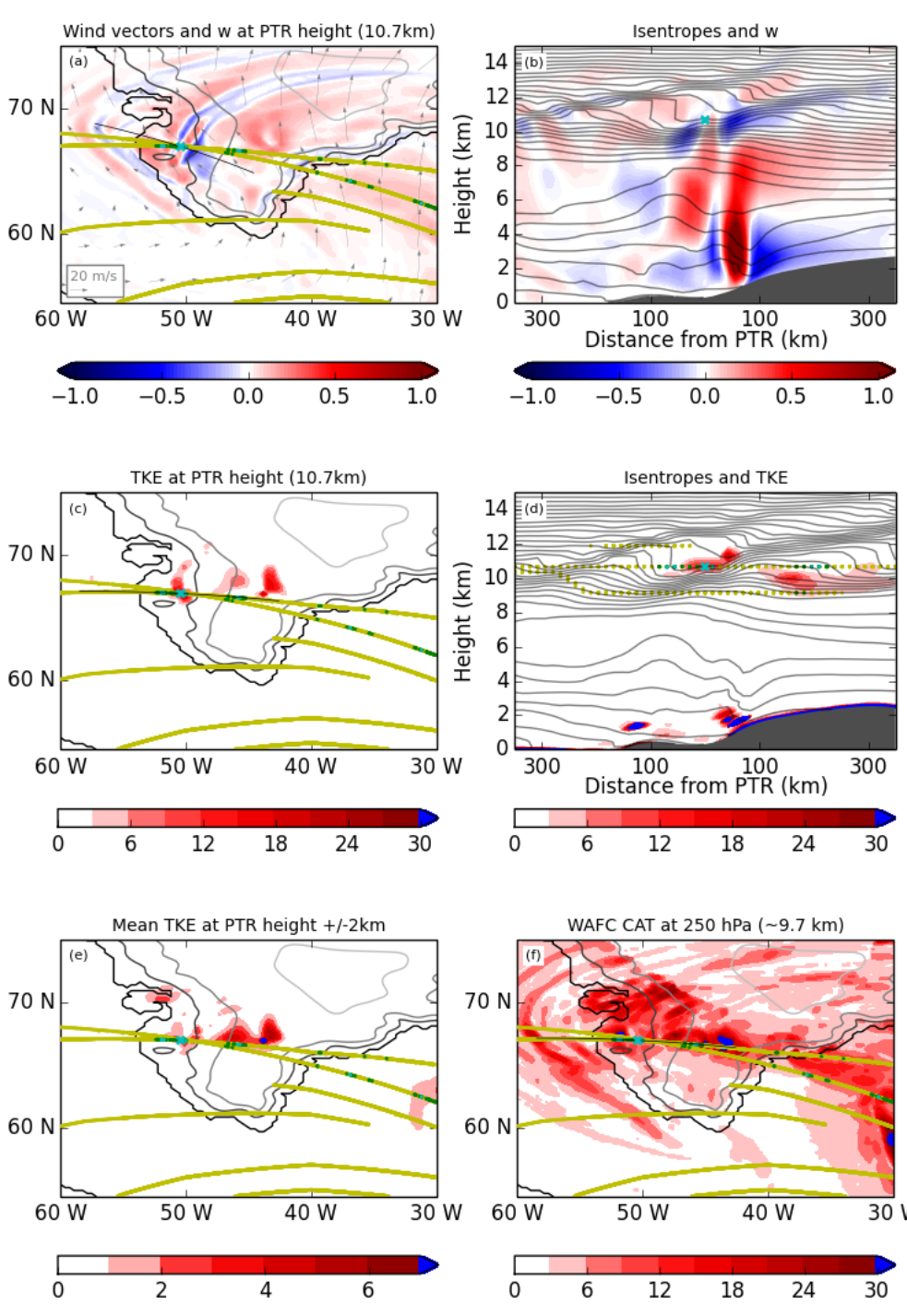

Figure 1: Model output and turbulence reports in the vicinity of the Case 1 turbu
reports over Greenland, at a time which is within an hour of the peak turbulence
report (PTR). Panel (a) shows model vertical velocity (w, colour shading), horizo
wind vectors, topographic height (contours) and turbulence reports (coloured do
10.7 km (the height of the PTR). Each turbulence report is represented by a colo

averaged between 8.7 km and 12.7 km, respectively. Panel (d) is a cross sectio the TKE diagnostic and potential temperature along a great circle roughly follow the track of the flight from which the PTR was taken. Coloured dots show the loc and severity (as in panel (a)) of those turbulence reports that are within 50 km o cross section. Panel (f) shows the WAFC CAT product at the nearest available pressure level to PTR height (250 hPa: a height of ~9.7 km at the PTR).

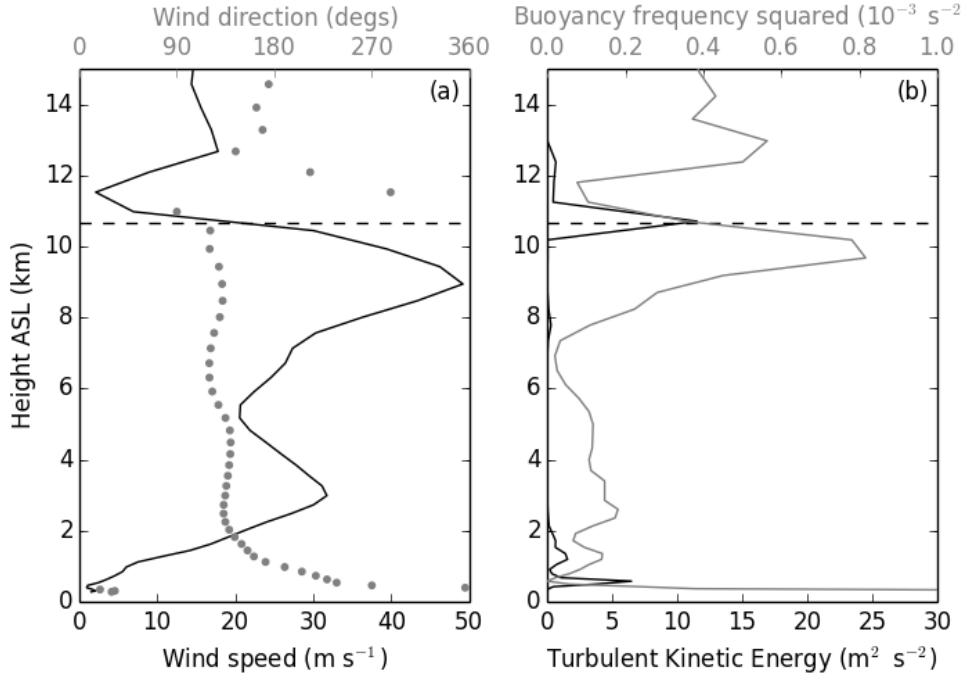

Figure 2: Vertical profiles of (a) wind speed and direction and (b) diagnosed TKI buoyancy frequency squared for Case 1, passing through the location of the pea turbulence report (the height of which is shown by the dashed line).

3.2 Case 2: Severe turbulence

During this case in March 2012 an aircraft encountered severe turbulence (maxi DEVG of 9.0 m s^{-1}) above Greenland's south west coast (see Figure 3). As in ca the synoptic situation was dominated by a low pressure system situated to the s of Greenland, forcing an easterly flow across southern Greenland. The turbulen reports indicate a region of instability above the steep slopes downwind of the Greenland plateau.

The global forecast wind profile for this case at the location of the turbulence ev shown in Figure 4(a). The buoyancy frequency profile is shown in Figure 4(b), revealing that the troposphere was, in general, stably stratified. The profiles indi the presence of a critical level with the wind turning through 180° between the surface and the stratosphere, with the sharpest change in wind direction near cr

strong ascent reminiscent of a hydraulic jump at low levels (below 4 km) and str
wind shear at upper levels (~9 km; Figure 4(a)) are indicative of wave breaking
turbulence. The TKE diagnostic captures the reported region of instability well, b
in the horizontal and vertical (Figure 3(c,d)). Such is the precision of this forecas
in this case the height-averaged TKE diagnostic (Figure 3(e)) adds no further
predictive value.

The WAFC CAT product (at 250 hPa and a little over an hour prior to this case's
PTR) gives an indication of widespread turbulence risk in the region with high ri
over the western edge of the Greenland plateau, but does not suggest a signific
risk at the location of the severe turbulence report above the steeper lee slopes
(Figure 3(f)). Again the WAFC CAT product indicates more widespread light
turbulence than was observed.

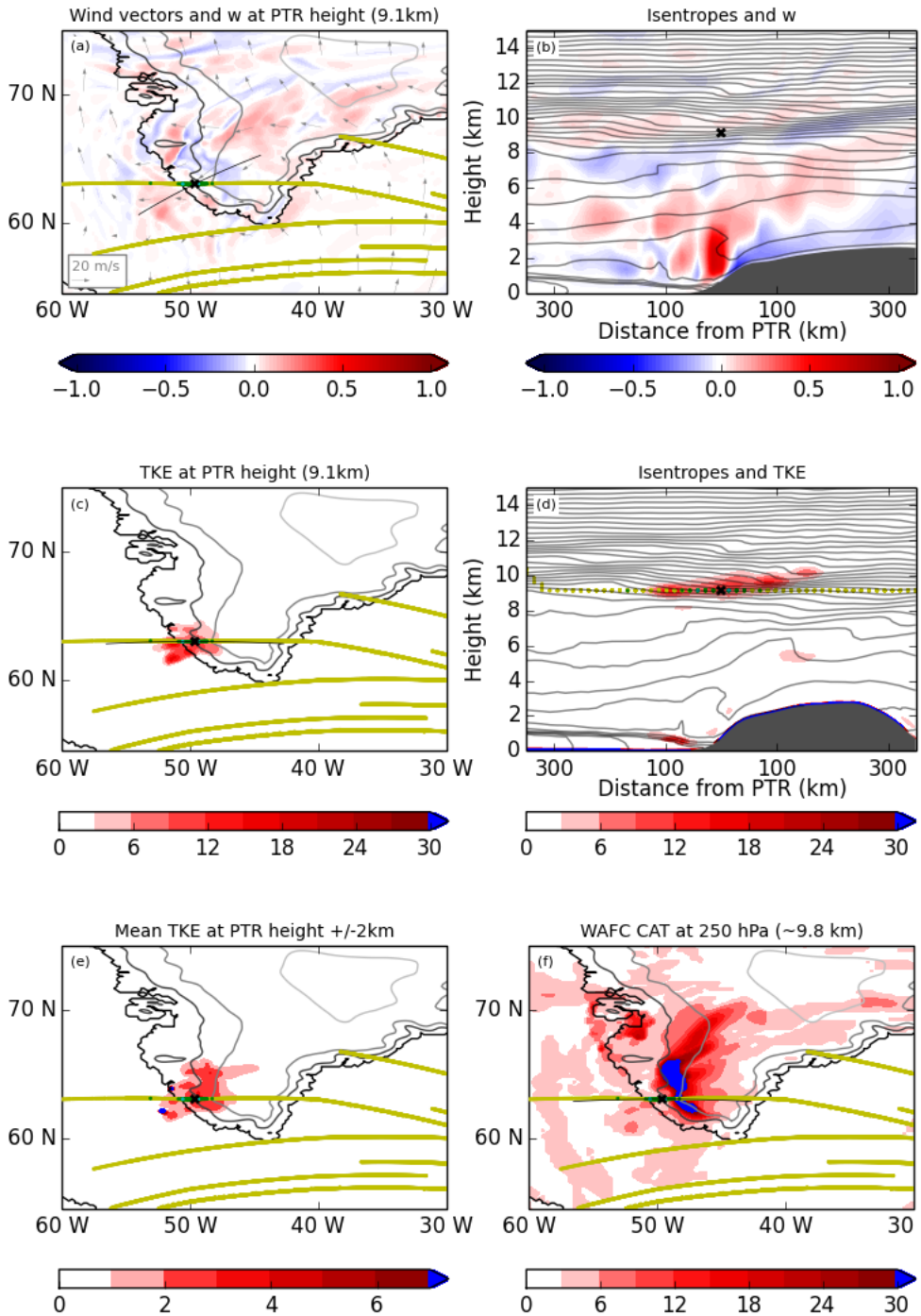

Figure 3: As in Figure 1, but for Case 2.

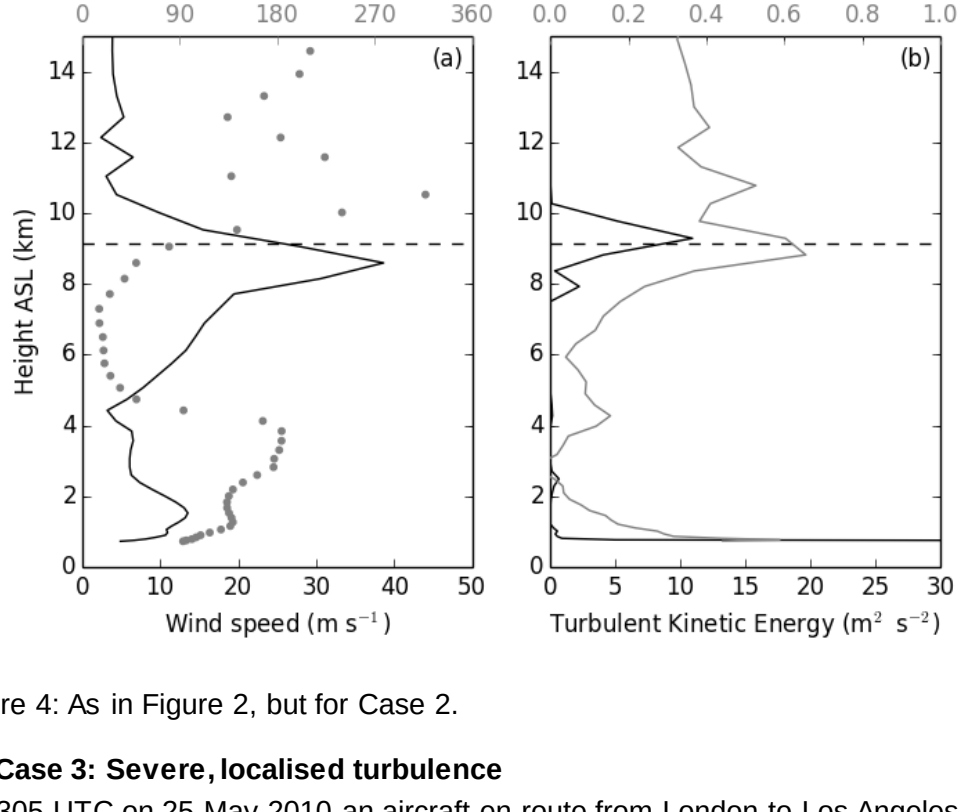

Figure 4: As in Figure 2, but for Case 2.

3.3 Case 3: Severe, localised turbulence

At 1305 UTC on 25 May 2010 an aircraft en route from London to Los Angeles encountered severe turbulence at 62.08°N, 48.29°W at ~10km elevation. This c has been studied in detail by Sharman et al. (2012) and the details of the severe turbulence encounter are taken from their paper. Figure 5 displays the location recorded turbulence event.

Over much of Greenland, high pressure and weak winds resided, but a strong easterly flow passed over the southern tip associated with a deep low pressure centre far to the south. The global model vertical profiles of wind speed and dire near the severe turbulence report are shown in Figure 6(a). These profiles are broadly consistent with those shown in Figure 3 of Sharman et al. (2012), indica an easterly flow at all altitudes and with a sudden drop in the wind speed above km. Analysis of model diagnostics (not shown) confirms the latter to be a result wave activity, associated with the upward growth in amplitude, steepening and apparent breaking of a vertically propagating mountain wave.

Figure 5(a) shows the modelled vertical velocity at observation height. Figure 5(shows a cross section of vertical velocity and potential temperature (which can compared with Figure 6 of Sharman et al.). Here, the wave steepening above 1 is clear in isentropes, with the drop in buoyancy frequency also evident in Figure 6(b). The Sharman et al. study included a 5 km horizontal resolution COAMPS simulation which indicated two regions of turbulence, one between 1 and 4 km a

Figure 5(c,d) shows that for this event the TKE diagnostic provides a very good, precise forecast of the location of the severe turbulence, and this turbulent regio corresponds closely to that diagnosed by the higher resolution model in Sharma al. Figure 5(f) shows the WAFC CAT forecast at 250 hPa at 12 UTC. As in Case this diagnostic gives an indication of turbulence risk near the southern tip of Greenland but again the turbulence forecast by the TKE diagnostic is considera more localised to the region of reported turbulence.

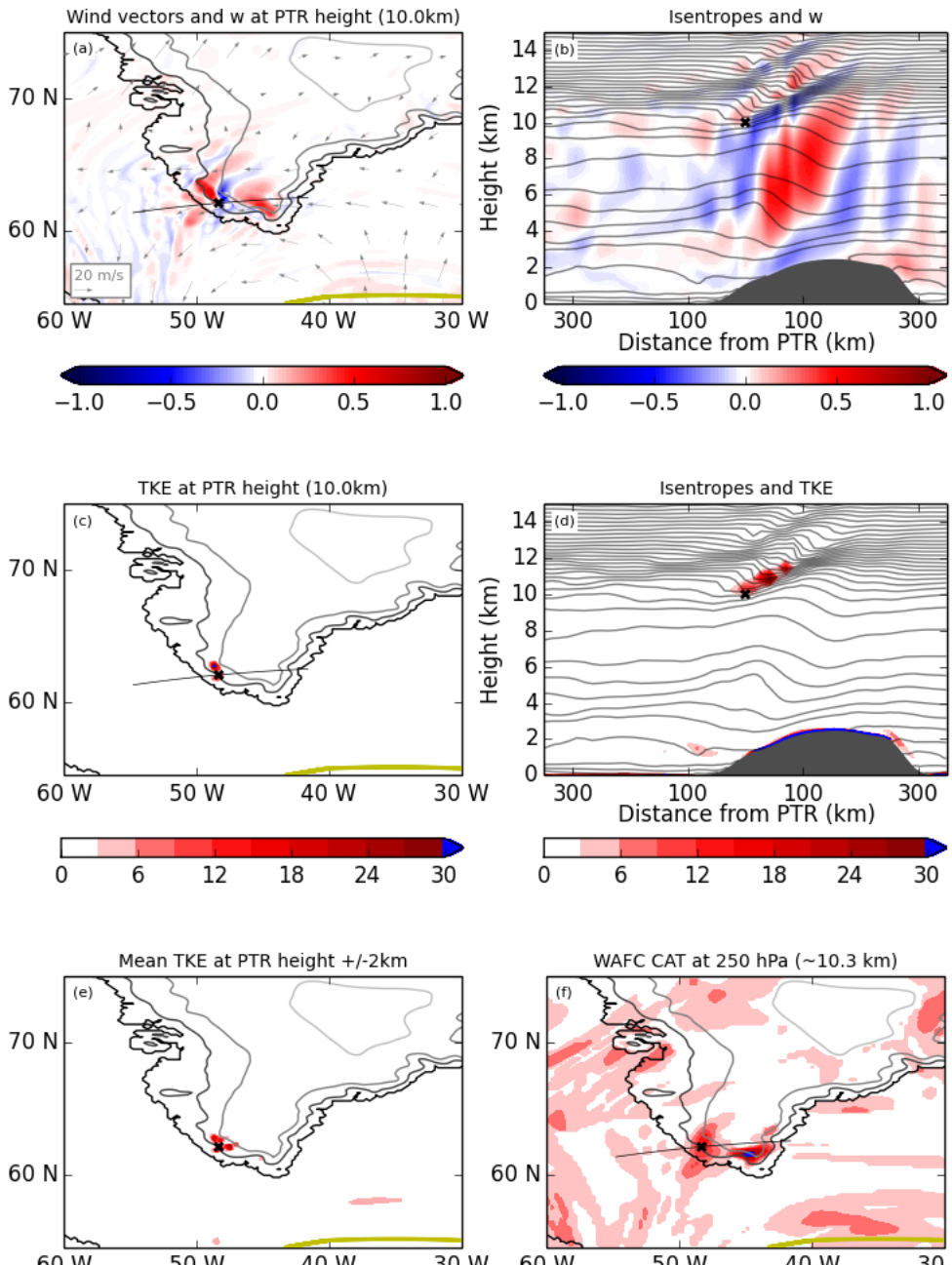

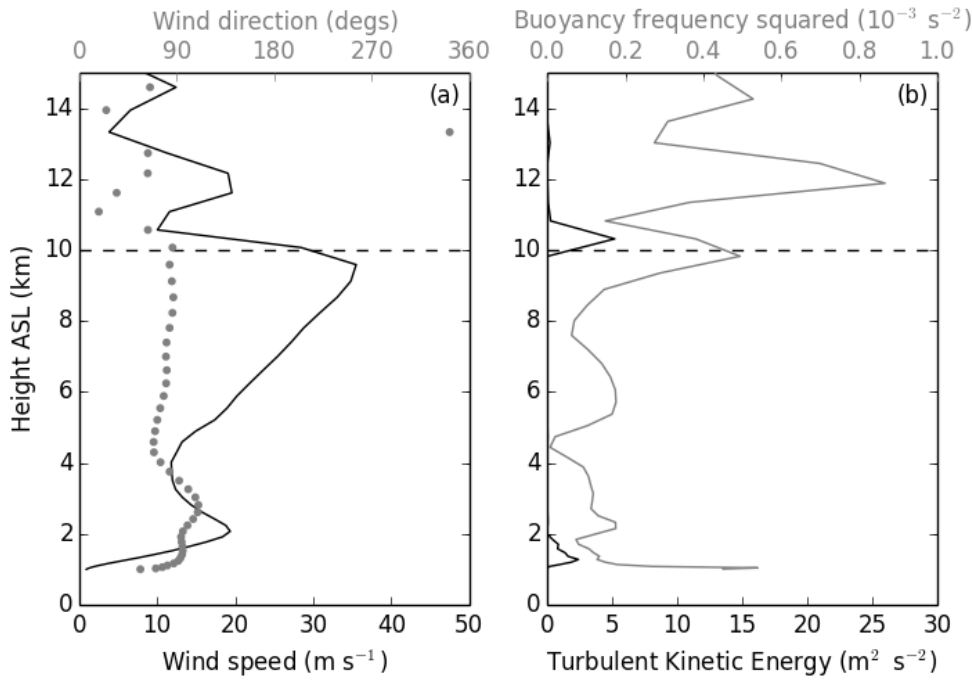

Figure 6: As in Figure 2, but for Case 3.

4. Long term verification

The case study analysis of Section 3 shows that the new TKE diagnostic is capa of forecasting regions of moderate to severe turbulence related to mountain wav activity over Greenland. In this section we explore whether this predictive skill h over longer time scales. During the 17-month period considered, moderate and severe turbulence events such as those discussed in Section 3 are rare occurre with reports of light turbulence more common, but quiescent conditions dominar Whether the new diagnostic is able to provide usable, meaningful forecasts of turbulence is clearly dependent on whether it is able to reliably identify both turbulence and the absence of turbulence.

Two TKE-derived turbulence risk diagnostics are trialled here as turbulence predictors: a spatial mean (TKE_{mean}), and spatial a maximum (TKE_{max}). The form the mean TKE value within the 100-km radius and 2-km deep cylinder centred o each report (see Figure 7), whilst the latter is the maximum TKE value within thi region. For each of these quantities, Table 1 shows mean values and standard deviations within three bins representing the severity of reported turbulence. Th are no turbulence (DEVG < 2), light turbulence (2 ≤ DEVG < 4.5) and moderate severe turbulence (DEVG ≥ 4.5). Reassuringly, both TKE_{mean} and TKE_{max} increa with successive levels of reported severity. Despite relatively large standard deviations within each bin, these positive correlations are statistically significant the 99 % level according to Welch's t-test.

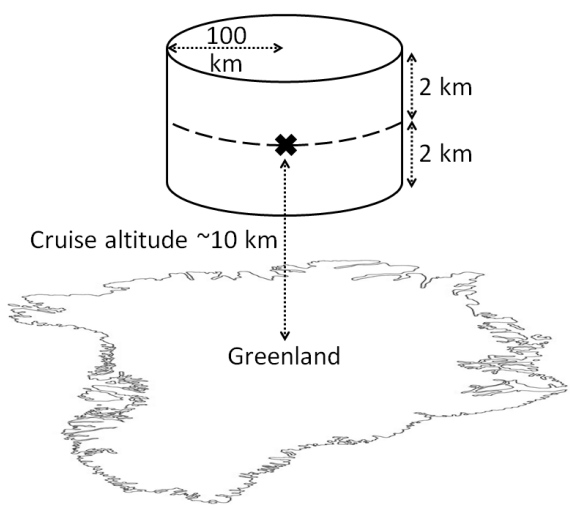

Figure 7: Schematic illustrating the model sampling region (cylinder) used in the calculation of mean and maximum modified TKE diagnostics for a single GADS observation (cross) in the long term verification.

To further assess the skill of the new turbulence predictor, a dichotomous verific approach is adopted, as regularly used in forecast verification including for the currently employed Met Office mountain CAT predictor (Turner, 1999). This app yields skill scores in the form of a forecast hit rate – the proportion of turbulence reports which are successfully forecast – and a false alarm rate – the proportion positive forecasts which are false. The combination of a large hit rate and a sma false alarm rate defines a good forecast product. To calculate these skill scores, necessary to transform our continuous datasets of observed DEVG and forecas into binary form (e.g. 1 = turbulence, 0 = no turbulence). For this, we define thresholds, both for DEVG and TKE. We set the former equal to the light turbule threshold of DEVG = 2 to test the ability of the new predictor to distinguish betw turbulent and quiescent conditions. The forecast TKE threshold is somewhat arbitrary, and so we arrive at this by assigning a value such that a prescribed, desired hit rate is achieved. We choose a hit rate of 80 %, and the assessment forecast skill is in the resulting false alarm rate.

Table 2(a) shows the frequency of positive and negative turbulence reports and forecasts (using TKE_{mean}), according to the criteria outlined above. This continge table is comprised of four elements – the 'joint distribution' – of which, reassurin the correct null forecasts and correct positive forecasts ('hits') have the greatest frequencies at 72 % and 15 % of the total number of reports respectively, whilst false positive ('false alarms'; 9 %) and false negative ('misses'; 4 %) forecasts y the lowest frequencies. These frequencies translate to a false alarm rate of 38 % presented in Table 3. Using TKE_{max} as the predictor yields a very similar result: false alarm rate of 39 %. The current WAFC CAT product yielded an optimum h false alarm rate combination of 40 % and 96 %, respectively, according to verific carried out in Turner (1999) which used a similar observation threshold at the

It should be noted that the choice of the 'long' stability function incorporated in t formulation of the TKE diagnostic (see Section 2) was subject to sensitivity testi the framework of this long term verification. Three different stability functions we trialled: the long tail function given in equation 3, a very long tail function which adapts equation (3) by replacing the 10 in the denominator with a 5, and a short function following Louis (1979). Of these three, the 'long' function trial was found deliver the greatest forecast skill score.

	No turbulence	Light turbulence	Moderate-severe turb.
Number of reports	2124	466	16
Mean TKE_{mean}	0.04	0.52	0.91
Std. TKE_{mean}	0.14	0.51	0.58
Mean TKE_{max}	1.7	16.1	28.8
Std. TKE_{max}	12.8	19.6	23.9

Table 1: TKE diagnostic statistics for varying reported turbulence severities.

	Reported 1 (DEVG ≥ 2)	Reported 0 (DEVG < 2)
Forecast 1 (TKE ≥ 0.085)	386 (15 %)	237 (9 %)
Forecast 0 (TKE < 0.085)	96 (4 %)	1887 (72 %)

Table 2: Contingency tables showing joint distributions of reported and pre turbulence where the forecast threshold is assigned such that the hit rate is 8 and the reported DEVG threshold is set to 2 (at the transition between null an turbulence).

	DEVG threshold = 2	
	Hit Rate	FA Rate
TKE_{mean}	80	38
TKE_{max}	80	39

Table 3: Hit and false alarm (FA) rates for TKE_{mean} and TKE_{max} using a reported DEVG threshold of 2.

5. Conclusions

This study has demonstrated that modern global NWP models are now sufficien advanced that they are able of representing a sufficient proportion of the gravity wave spectrum to diagnose mountain wave turbulence. This represents a major breakthrough in NWP performance in mountainous regions, and forecasts of mountain CAT are no longer dependent on a sophisticated mountain-wave parametrization. A TKE diagnostic, derived from a mixing coefficient with a long stability tail, has demonstrated skill in the prediction of mountain CAT, both in th

weak mountain wave activity, with a reversal of mean-state flow direction in the stratosphere coinciding with a reported region of turbulence peaking at severe. single severe turbulence report in Case 3 corresponds to a large amplitude verti propagating wave in the model. In all three cases, both the new diagnosed TKE the current WAFC CAT diagnostic give a good indication of the risk of turbulenc the locations of positive reports. However, the TKE diagnostic consistently provi more localized and precise forecast of turbulence, whilst the WAFC CAT diagno indicates more widespread turbulence than was observed. In other words, in ea these cases the TKE diagnostic demonstrates superior skill than the current operational product, and produces forecasts that would have provided greater v to pilots.

In the long term objective verification, the TKE diagnostic is shown to provide a indication of turbulence risk over an extended period of time (17-month). Here, t skill demonstrated is in picking out rare turbulence events within a large dataset dominated by low turbulence conditions. Trialling both a neighbourhood spatial and maximum of the diagnostic, a forecast hit rate of 80 % is achievable with a alarm rate less than 40 %. This represents a marked improvement on the performance of the current mountain wave predictor. Little demonstrable differe forecast skill is found between the spatial mean and spatial maximum products. should also be noted that skill scores may be dependent on the ratio of null to positive reports, and that in this study this ratio was reduced for computational reasons.

It should be noted that there are alternative derivations for TKE. For example, in MetUM, turbulence closure is handled using a turbulence timescale (Lock et al., 2016), as opposed to a predefined mixing length as implemented in the TKE derivation used in the present study. However, since the purpose of the mounta CAT predictor is to provide turbulence warnings at appropriate thresholds, the d of its derivation are not pertinent.

The skill of operational forecasts of mountain turbulence has, until recently, bee limited due to its dependence on a parameterization scheme that, due to its tuni and inherent simplifications in its formulation, is poorly suited to this purpose. Th demonstrated predictive skill of a turbulence diagnostic derived directly from the output of an operational global model (the new MetUM global model with ENDG dynamics) has clear implications for the mitigation of the turbulence hazard, and points towards the future of mountain turbulence forecasting for aviation. Future development and improvement of 'resolved' model forecasting of mountain turbulence would benefit from a deeper understanding of the interactions betwe mountain waves, the mean flow in which they propagate, and the turbulence the generate upon breaking. To facilitate this, additional direct measurements of TK breaking gravity waves, although difficult and hazardous to obtain, would be of g benefit.

References

Clark TL and Peltier WR. 1977. On the evolution and stability of finite-amplitude mountain waves. *J. Atmos. Sci.*, **34**, 1715-1730.

Davies T, Cullen MJP, Malcolm AJ, Mawson MH, Staniforth A, White AA and W N. 2005. A new dynamical core for the Met Office's global and regional modellin the atmosphere. *Quart. J. Roy. Met. Soc.*, **131**, 1759-1782.

Elvidge AD, Renfrew IA, King JC, Orr A and Lachlan-Cope TA. 2016. Foehn wa distributions in nonlinear and linear flow regimes: a focus on the Antarctic Penin *Q. J. R. Meteorol. Soc.*, doi: 10.1002/qj.2489.

Ellrod GP and Knapp DI. 1992. An Objective Clear Air Turbulence Forecasting Technique: Verification and Operational Use. *Weather Forecasting*, vol. 7, pp 15 165.

Gill PG and Stirling AJ. 2013. Including convection in global turbulence forecast *Meteorol. Appl.*, **20**, 107-114.

Grubišić V, Doyle JD, Kuttner J, Mobbs S, Smith RB, Whiteman CD, Dirks R, Cz S, Cohn SA, Vosper S and Weissmann M. 2008. The Terrain-Induced Rotor Experiment: A field campaign overview including observational highlights. *Bulle the American Meteorological Society*, **89**(10), p.1513.

Jiang Q and Doyle JD. 2004. Gravity wave breaking over the Central Alps: Role complex terrain. *J. Atmos. Sci.*, **64**, 2249-2266.

Lane TP, Doyle JD, Sharman RD, Shapiro MA and Watson CD. 2009. Statistics dynamics of aircraft encounters of turbulence over Greenland. *Mon. Wea. Rev.* 2687-2702.

Lilly DK. 1978. A severe downslope windstorm and aircraft turbulence event ind by a mountain wave. *J. Atmos. Sci.,* **35**, 59–77, doi: 10.1175/1520-0469(1978)035<0059:ASDWAA>2.0.CO;2.

Lock AP, Edwards J, Boutle I. 2016. The Parametrization of Boundary Layer Processes. *Unified Model documentation paper*, **71**.

Melvin T, Dubal M, Wood N, Staniforth A and Zerroukat M. 2010. An inherently mass-conserving semi-implicit semi-Lagrangian discretisation of the nonhydrost vertical slice equations. *Quart. J. Roy. Meteorol. Soc.,* **136**, 799–814.

Mobbs SD, Vosper SB, Sheridan PF, Cardoso R, Burton RR, Arnold SJ, Hill MK Horlacher V, Gadian AM. 2005. Observations of downslope winds and rotors in Falkland Islands. *Quart. J. Roy. Meteorol. Soc.,* **131**, 329-51.

Smith RB. 1987. Aerial observations of the Yugoslavian Bora. *J. Atmos. Sci.*, **44** 269–297, doi: 10.1175/1520-0469(1987)044<0269:AOOTYB>2.0.CO;2.

Strauss L, Serafin S, Haimov S and Grubišić V. 2015. Turbulence in breaking mountain waves and atmospheric rotors estimated from airborne in situ and Dop radar measurements. *Quart. J. Roy. Met. Soc.*, **141**, 3207-3225.

Teixeira, MA and Miranda, PM. 2009. On the momentum fluxes associated with mountain waves in directionally sheared flows. *J. Atmos. Sci.*, **66**, 3419-3433.

Truscott BS. 2000. EUMETNET AMDAR AAA AMDAR Software Developments Technical Specification. Doc. Ref. E_AMDAR/TSC/003

Turner J. 1999. Development of a mountain wave turbulence prediction scheme civil aviation. *Met Office Forecasting Technical Report*, No. 265.

Webster S, Brown AR, Cameron DR and Jones CP. 2003. Improving the representation of orography in the Met Office Unified Model. *Quart. J. Roy. Mete Soc.,* **129**, 1989-2010.

Vosper, SB. 2015. Mountain waves and wakes generated by South Georgia: implications for drag parametrization. *Quart. J. Roy. Meteorol. Soc.*, **141**, 2813-2

Wobrock W, Flossmann AI, Colvile RN and Inglis DWF. 1997. Modelling of air fl and cloud fields over the Northern Pennines. *Atmospheric Environment*, **31**(16), 2421-2439.

Wolff JK and Sharman RD. 2008. Climatology of upper-level turbulence over the continental United States. *J. Appl. Meteor. Climatol.*, **47**, 2198-2214.

Wood N, Staniforth A, White AA, Allen T, Diamantakis M, Gross M, Melvin T, Sm C, Vosper SB, Zerroukat M and Thuburn J. An inherently mass-conserving sem implicit semi-Lagrangian discretisation of the deep-atmosphere global nonhydro equations. Submitted to *Quart. J. Roy. Meteorol. Soc*.